Astronomy
&
Astrophysics

HST color-magnitude diagrams of 74 galactic globular clusters in the HST $F439W$ and $F555W$ bands[⋆]

G. Piotto[1], I. R. King[2], S. G. Djorgovski[3], C. Sosin[2], M. Zoccali[4], I. Saviane[5], F. De Angeli[1,2], M. Riello[1,6], A. Recio Blanco[1], R. M. Rich[7], G. Meylan[8], and A. Renzini[4]

[1] Dipartimento di Astronomia – Università di Padova, 35122 Padova, Italy
    e-mail: `piotto@pd.astro.it; deangeli@pd.astro.it; recio@pd.astro.it`
[2] Astronomy Department, University of California, Berkeley, CA 94720, USA
    e-mail: `king@glob.berkeley.edu; craig@sosin.org`
[3] California Institute of Technology, MS 105-24, Pasadena, CA 91125, USA
    e-mail: `george@deimos.caltech`
[4] European Southern Observatory, 85748 Garching bei Munich, Germany
    e-mail: `mzoccali@eso.org; gmeylan@eso.org; arenzini@eso.org`
[5] European Southern Observatory, Casilla 19001, Santiago, Chile
[6] Osservatorio Astronomico, 35122 Padova, Italy
    e-mail: `riello@pd.astro.it`
[7] Physics and Astronomy Department, University of California, Los Angeles, CA 90024, USA
    e-mail: `rmr@astro.ucla.edu`
[8] Space Telescope Science Institute, Baltimore, MD 21218, USA

Abstract. We present the complete photometric database and the color-magnitude diagrams for 74 Galactic globular clusters observed with the HST/WFPC2 camera in the $F439W$ and $F555W$ bands. A detailed discussion of the various reduction steps is also presented, and of the procedures to transform instrumental magnitudes into both the HST $F439W$ and $F555W$ flight system and the standard Johnson B and V systems. We also describe the artificial star experiments which have been performed to derive the star count completeness in all the relevant branches of the color magnitude diagram. The entire photometric database and the completeness function will be made available on the Web immediately after the publication of the present paper.

1. Introduction

Because of its excellent resolving power, the *Hubble Space Telescope* offers an exceptional opportunity to study the crowded centers of Galactic globular clusters (GGC). We therefore began several years ago a study of color–magnitude diagrams (CMD) of clusters, using HST's WFPC2 camera.

Our first program, GO-6095, examined 10 clusters in the HST B ($F439W$) and V ($F555W$) bands (Sosin et al. 1997a; Piotto et al. 1997), with accompanying ultraviolet images for better study of the extended blue tails that occur on the horizontal branches (HB) of a number of clusters. That program gave some quite interesting results, like the first discovery of

extended horizontal branches (EHB) in the metal-rich clusters NGC 6388 and NGC 6441 (Rich et al. 1997), and the discovery in NGC 2808 of an EHB extending down the helium-burning main sequence, with a multimodal distribution of stars along it (Sosin et al. 1997b). GO-6095 also persuaded us that it would be more profitable to explore a larger number of clusters more rapidly in B and V alone, in order to delineate the upper parts of their CMDs, and especially their HBs, with the intention of returning to the more interesting clusters for more intensive follow-up studies. We therefore changed our program to a snapshot study (GO-7470) aimed at producing CMDs down to a little below the main-sequence (MS) turnoff for all Galactic globular clusters with apparent B distance modulus ≤18.0 and whose centers had not yet been observed by HST in a comparable way – 53 clusters in all. Since snapshot programs have no guarantee of being completed in a given year, we have resubmitted each year the list of clusters not yet observed (GO-8118, GO-8723). By the time we are writing this paper,

only one of the GGCs in our original list remains to be observed: NGC 6779. There were also in the HST archive images of a number of clusters that could be treated similarly. We have measured these in the same way as our own images, and present here CMDs of a total of 74 GGCs, measured and reduced in a uniform way, all observed with WFPC2 with the same filter set, and with the PC centered on the cluster center. For all of the 74 GGCs, we ran artificial star experiments to measure the completeness of the star counts in all the relevant branches of the CMD. In this paper we describe the observations, the reduction procedures, the artificial star tests, and the steps followed to transform the instrumental magnitudes into magnitudes in both the HST flight and standard Johnson photometric systems.

The data set that we present has already been shown to be extremely valuable in attacking a number of still-open topics on evolved stars in GGCs. In particular, these data have been used by Piotto et al. (1999a) to investigate the problem of the EHBs and by Raimondo et al. (2002) to study the properties of the red HB in metal-rich clusters; in Zoccali et al. (1999) and Bono et al. (2001) we have throughly discussed the red giant branch (RGB) bump, and compared the predicted position and dimension of this feature with the observed ones; in Zoccali et al. (2000) we have used the star counts on the HB and on the RGB to gather information on the helium content and on the dependence of the helium content on the cluster metallicity; in Zoccali & Piotto (2000) we have made the most extensive comparison so far available between the model evolutionary times away from the main sequence and the actual star counts on the subgiant branch (SGB) and RGB; in Cassisi et al. (2001) we have compared the observed and theoretical properties of the asymptotic giant branches; in Piotto et al. (2000) we have used the CMDs in our database for the study of the GGC relative ages, and, finally, in Piotto et al. (1999b), we have started to investigate the GGC blue straggler (BS) population, and have shown how the BS CMD and luminosity function can differ in clusters with rather different morphologies. Future papers will carry out other detailed studies based on the same data. Among these, we are presently working on the derivation of the relative ages, following the strategy already delineated in Rosenberg et al. (1999) on a similarly photometrically homogeneous set of CMDs, but from ground-based data, and by Piotto et al. (2000) on a small subsample of the present HST database. We are also working on the large BS database that came from the CMDs presented in the following sections (Piotto et al. 2002, in preparation).

As better described in Sect. 3, all the CMDs, the star positions, the magnitudes in both the $F439W$ and $F555W$ flight system, and the B and V standard Johnson system will be made available to the astronomical community immediately after the publication of the present paper.

2. Observations, reductions and calibrations

2.1. Pre-reduction of the images

All the photometric data for the 74 GGCs presented in this paper come from HST/WFPC2 observations in the $F439W$ and

Table 1. Observation log. Asterisks indicate clusters reduced by using Stetsons PSFs.

Cluster	Program ID	Exp. Time $F555W$ [s]	Exp. Time $F439W$ [s]
NGC 104	GO6095	1, 7	7, 2 × (50)
NGC 362	GO6095	3, 18	18, 2 × (160)
NGC 1261*	GO7470	10, 40	40, 2 × (160)
NGC 1851	GO6095	6, 40	40, 2 × (160)
NGC 1904	GO6095	7, 40	40, 2 × (160)
NGC 2419*	archive	10, 2 × (100)	2 × (260)
NGC 2808	GO6095	7, 50	50, 2 × (230)
NGC 3201*	GO8118	3, 2 × (30)	40, 2 × (100)
NGC 4147*	GO7470	10, 40	40, 2 × (160)
NGC 4372	GO8118	3, 2 × (30)	40, 2 × (100)
NGC 4590*	GO7470	5, 40	40, 2 × (100)
NGC 4833	GO8118	3, 2 × (30)	40, 2 × (100)
NGC 5024	GO8118	5, 40	40, 2 × (160)
NGC 5634	GO7470	10, 40	40, 2 × (160)
NGC 5694	archive	10, 4 × (60)	120, 3 × (500)
IC 4499*	GO8723	10, 40	40, 2 × (160)
NGC 5824	archive	2 × (10), 5 × (60)	120, 3 × (500)
NGC 5904	GO8118	3, 2 × (30)	40, 2 × (100)
NGC 5927	GO6095	10, 50	50, 2 × (160)
NGC 5946*	GO7470	10, 40	40, 2 × (160)
NGC 5986*	GO7470	10, 40 ec	40, 2 × (160)
NGC 6093*	archive	2 × (2), 4 × (23)	2 × (30)
NGC 6139	GO7470	10, 40	40, 2 × (160)
NGC 6171*	GO7470	5, 40	40, 2 × (100)
NGC 6205*	archive	4 × (1), 4 × (8)	2 × (14)
NGC 6229	GO8118	10, 40	40, 2 × (160)
NGC 6218	GO8118	3, 2 × (30)	40, 2 × (100)
NGC 6235	GO7470	10, 40	40, 2 × (160)
NGC 6256*	GO7470	10, 40	40, 2 × (160)
NGC 6266	GO8118	3, 2 × (30)	40, 2 × (100)
NGC 6273	GO7470	10, 40	40, 2 × (160)
NGC 6284*	archive	4, 4 × (40)	30, 6 × (160)
NGC 6287*	archive	2 × (5), 3 × (50)	60, 230
		3 × (1000)	
NGC 6293	archive	2, 5 × (40)	20, 6 × (160)
NGC 6304*	GO7470	10, 40	40, 2 × (160)
NGC 6316*	GO7470	10, 40	40, 2 × (160)
NGC 6325*	GO7470	10, 40	40, 2 × (160)
NGC 6342	GO7470	10, 40	40, 2 × (160)
NGC 6356	GO7470	10, 40	40, 2 × (160)
NGC 6355*	GO7470	10, 40	40, 2 × (160)
IC 1257*	GO8723	30, 100	160, 2 × (300)
NGC 6362*	GO7470	5, 40	40, 2 × (100)
NGC 6380	GO7470	10, 40	40, 2 × (160)
NGC 6388	GO6095	12, 50	50, 2 × (160)
NGC 6402	GO8118	7, 40	40, 2 × (160)
NGC 6401	GO7470	10, 40	40, 2 × (160)
NGC 6397*	archive	1, 8, 6 × (40)	2 × (10), 2 × (80)
			16 × (400), 4 × (500)
NGC 6440*	GO8723	10, 40	40, 2 × (160)
NGC 6441	GO6095	14, 50	50, 2 × (160)
NGC 6453	GO8118	10, 40	40, 2 × (160)
NGC 6517*	GO8723	10, 40	40, 2 × (160)
NGC 6522	GO6095	10, 50	50, 2 × (160)
NGC 6539	GO8118	10, 40	40, 2 × (160)
NGC 6540	GO8118	5, 40	40, 2 × (160)
NGC 6544	GO8118	3, 2 × (30)	40, 2 × (100)
NGC 6569	GO8118	5, 40	40, 2 × (160)
NGC 6584	GO8118	5, 2 × (30)	40, 2 × (100)

Table 1. continued.

Cluster	Program ID	Exp. Time $F555W$ [s]	Exp. Time $F439W$ [s]
NGC 6624	archive	4 × (10)	2 × (50)
NGC 6638	GO8118	5, 40	40, 2 × (160)
NGC 6637	GO8118	3, 2 × (30)	40, 2 × (100)
NGC 6642	GO8118	3, 40	40, 2 × (160)
NGC 6652*	GO6095	10, 50	50, 2 × (160)
NGC 6681*	GO8723	3, 2 × (30)	40, 2 × (100)
NGC 6712*	archive	60	160
NGC 6717	GO8118	3, 2 × (30)	40, 2 × (100)
NGC 6723	GO8118	3, 2 × (30)	40, 2 × (100)
NGC 6760*	GO8723	7, 40	40, 2 × (160)
NGC 6838	GO8118	3, 2 × (30)	40, 2 × (100)
NGC 6864*	GO8723	7, 40	40, 2 × (160)
NGC 6934*	GO7470	10, 40	40, 2 × (160)
NGC 6981	GO7470	10, 40	40, 2 × (160)
NGC 7078	archive	4 × (8)	2 × (40)
NGC 7089	GO8118	3, 2 × (30)	40, 2 × (100)
NGC 7099	archive	4 × (4)	2 × (40)

$F555W$ bands; in all cases, the PC camera was centered on the cluster center. Table 1 list the observed clusters (Col. 1), the origin of the observations (Col. 2), and the exposure times in $F555W$ (Col. 3) and $F439W$ (Col. 4) bands. Table 2 give a few relevant parameters (from the Harris 1996 compilation) Fig. 1 shows the spatial distribution of the target clusters within the Galaxy.

After the snapshot observations (or, for 12 clusters, after the public release date), the images were retrieved via ftp from the HST archive in Baltimore, and they were furtherly processed partially following the recipe in Silbermann et al. (1996). As in Silbermann et al., the vignetted pixels, and bad pixels and columns, were masked out using a vignetting frame created by P. B. Stetson, together with the appropriate data-quality file for each frame. However, we did *not* correct for the pixel area map, since this correction is included in the calibration process described below. Finally the single-chip frames were extracted from the 4-chip-stack files, and analyzed separately. Frames obtained both at gain = 7 e⁻/ADU and at 15 e⁻/ADU were available, so care was taken to adjust the various parameters to the applicable gain value for each image.

2.2. Instrumental magnitudes

The photometric reduction was carried out using the DAOPHOTII/ALLFRAME package (Stetson 1987, 1994). Preliminary photometry was carried out in order to construct an approximate list of stars for each single frame. This list was used to match the different frames accurately. With the correct coordinate transformations among the frames, we obtained a single image, combining all the frames, regardless of the filter. In this way we could eliminate all the cosmic rays and obtain the highest signal/noise image for star finding. We ran the
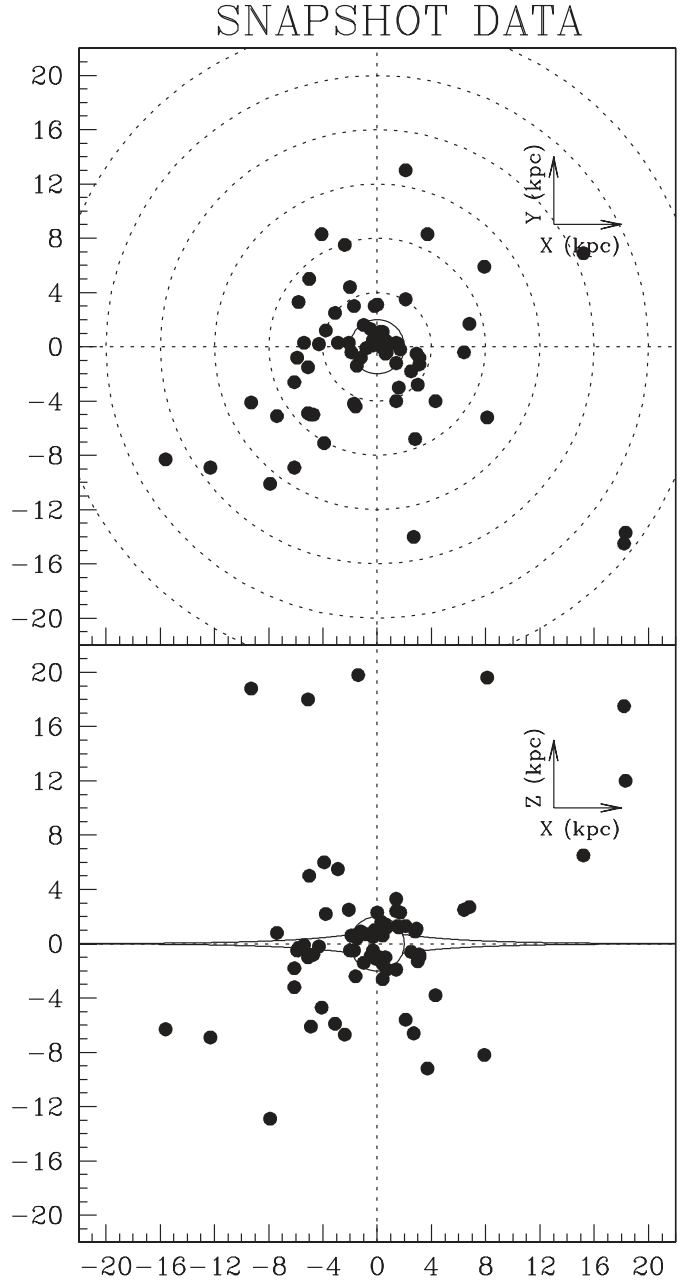

Fig. 1. Spatial distribution of the target clusters within the Galaxy.

DAOPHOT/FIND routine on the stacked image and performed PSF-fitting photometry in order to obtain the deepest list of stellar objects free from spurious detections. The subtracted image was searched again for objects missed in the first pass, and the new list was appended to the existing one. Finally, the entire star list was given as input to ALLFRAME, for the simultaneous PSF-fitting photometry of all the individual frames. In some cases we could not construct a PSF from our images, since there were not enough sufficiently isolated stars in any of the four chips. In those instances, the PSFs used were the high-S/N PSFs extracted by P. B. Stetson (private communication) from a large set of uncrowded and unsaturated WFPC2 images. The clusters for which Stetson PSFs have been used are marked with an asterisk in Table 1. For each of the WFPC2 chips, the (typically two) $F555W$ and (typically three) $F439W$ magnitude

Table 2. Main parameters of the clusters: Cols. 1 and 2 give the cluster identification number and other commonly used cluster name, Cols. 3 and 4 the Galactic longitude and latitude (degrees), Col. 5 gives the distance from the Galactic center (kpc), assuming $R_0 = 8.0$ kpc, Col. 6 the foreground reddening, Col. 7 the apparent visual distance modulus, Col. 8 the absolute visual magnitude, Col. 9 the metallicity [Fe/H], Col. 10 the central concentration ($c = \log(r_t/r_c)$, a "c" denotes a core-collapsed cluster), Col. 11 the logarithm of core relaxation time (log (years)), Col. 12 the logarithm of relaxation time at the half-mass radius (log (years)), Col. 13 the logarithm of central luminosity density ($L_\odot$ pc^{-3}).

ID	Name	l	b	R_{GC}	$E(B-V)$	$(m-M)_V$	M_{Vt}	[Fe/H]	c	r_t	$\log t_c$	$\log t_h$	$\log \rho_0$
NGC 104	47 Tuc	305.90	−44.89	7.4	0.04	13.37	−9.42	−0.76	2.03	47.25	8.06	9.48	4.77
NGC 362		301.53	−46.25	9.3	0.05	14.80	−8.40	−1.16	1.94c:	16.11	7.76	8.92	4.70
NGC 1261		270.54	−52.13	18.2	0.01	16.10	−7.81	−1.35	1.27	7.28	8.74	9.20	2.96
NGC 1851		244.51	−35.04	16.7	0.02	15.47	−8.33	−1.22	2.32	11.70	6.98	8.85	5.32
NGC 1904	M 79	227.23	−29.35	18.8	0.01	15.59	−7.86	−1.57	1.72	8.34	7.78	9.10	4.00
NGC 2419		180.37	25.24	91.5	0.11	19.97	−9.58	−2.12	1.40	8.74	9.96	10.55	1.54
NGC 2808		282.19	−11.25	11.0	0.23	15.56	−9.36	−1.15	1.77	15.55	8.28	9.11	4.61
NGC 3201		277.23	8.64	9.0	0.21	14.24	−7.49	−1.58	1.30	28.45	8.81	9.23	2.69
NGC 4147		252.85	77.19	21.3	0.02	16.48	−6.16	−1.83	1.80	6.31	7.49	8.67	3.48
NGC 4372		300.99	−9.88	7.1	0.39	15.01	−7.77	−2.09	1.30	34.82	8.90	9.59	2.09
NGC 4590	M 68	299.63	36.05	10.1	0.05	15.19	−7.35	−2.06	1.64	30.34	8.67	9.29	2.54
NGC 4833		303.61	−8.01	6.9	0.33	14.92	−8.01	−1.79	1.25	17.85	8.71	9.34	3.06
NGC 5024	M 53	332.96	79.76	18.8	0.02	16.38	−8.77	−1.99	1.78	21.75	8.79	9.69	3.04
NGC 5634		342.21	49.26	21.9	0.05	17.22	−7.75	−1.82	1.60	8.36	8.61	9.28	3.12
NGC 5694		331.06	30.36	29.1	0.09	17.98	−7.81	−1.86	1.84	4.29	7.86	9.15	4.03
IC 4499		307.35	−20.47	15.7	0.23	17.09	−7.33	−1.60	1.11	12.35	9.37	9.66	1.49
NGC 5824		332.55	22.07	25.8	0.13	17.93	−8.84	−1.85	2.45	15.50	7.88	9.33	4.66
NGC 5904	M 5	3.86	46.80	6.2	0.03	14.46	−8.81	−1.29	1.83	28.40	8.26	9.53	3.91
NGC 5927		326.60	4.86	4.5	0.45	15.81	−7.80	−0.37	1.60	16.68	8.29	8.98	3.87
NGC 5946		327.58	4.19	7.4	0.54	17.21	−7.60	−1.38	2.50c	24.03	7.06	8.95	4.50
NGC 5986		337.02	13.27	4.8	0.27	15.94	−8.42	−1.58	1.22	10.52	8.94	9.23	3.30
NGC 6093	M 80	352.67	19.46	3.8	0.18	15.56	−8.23	−1.75	1.95	13.28	7.73	8.86	4.76
NGC 6139		342.37	6.94	3.6	0.75	17.35	−8.36	−1.68	1.80	8.52	7.56	9.04	4.66
NGC 6171	M 107	3.37	23.01	3.3	0.33	15.06	−7.13	−1.04	1.51	17.44	8.05	9.31	3.13
NGC 6205	M 13	59.01	40.91	8.7	0.02	14.48	−8.70	−1.54	1.51	25.18	8.80	9.30	3.33
NGC 6229		73.64	40.31	30.0	0.01	17.46	−8.07	−1.43	1.61	5.38	8.36	9.19	3.40
NGC 6218	M 12	15.72	26.31	4.5	0.19	14.02	−7.32	−1.48	1.39	17.60	8.10	9.02	3.23
NGC 6235		358.92	13.52	2.9	0.36	16.11	−6.14	−1.40	1.33	7.61	8.11	8.67	3.11
NGC 6256		347.79	3.31	2.1	1.03	17.31	−6.02	−0.70	2.50c	7.59	5.36	8.40	5.70
NGC 6266	M 62	353.58	7.32	1.7	0.47	15.64	−9.19	−1.29	1.70c:	8.97	7.64	9.19	5.14
NGC 6273	M 19	356.87	9.38	1.6	0.37	15.85	−9.08	−1.68	1.53	14.50	8.50	9.34	3.96
NGC 6284		358.35	9.94	6.9	0.28	16.70	−7.87	−1.32	2.50c	23.08	7.15	9.16	4.44
NGC 6287		0.13	11.02	1.7	0.60	16.51	−7.16	−2.05	1.60	10.51	7.85	8.66	3.85
NGC 6293		357.62	7.83	1.4	0.41	15.99	−7.77	−1.92	2.50c	14.23	6.24	8.91	5.22
NGC 6304		355.83	5.38	2.1	0.52	15.54	−7.32	−0.59	1.80	13.25	7.38	8.89	4.39
NGC 6316		357.18	5.76	3.2	0.51	16.78	−8.35	−0.55	1.55	5.93	7.72	9.00	4.21
NGC 6325		0.97	8.00	2.0	0.89	17.68	−7.35	−1.17	2.50c	9.49	5.94	8.92	5.40
NGC 6342		4.90	9.73	1.7	0.46	16.10	−6.44	−0.65	2.50c	14.86	6.09	8.66	4.77
NGC 6356		6.72	10.22	7.6	0.28	16.77	−8.52	−0.50	1.54	7.97	8.33	9.26	3.76
NGC 6355		359.58	5.43	1.0	0.75	16.62	−7.48	−1.50	2.50c	15.18	5.95	8.71	4.95
IC 1257		16.53	15.14	17.9	0.73	19.25	−6.15	−1.70					
NGC 6362		325.55	−17.57	5.3	0.08	14.79	−7.06	−0.95	1.10	16.67	9.07	9.31	2.22
NGC 6380	Ton 1	350.18	−3.42	3.2	1.17	18.77	−7.46	−0.50	1.55c:	12.06	8.39	8.87	3.70
NGC 6388		345.56	−6.74	4.4	0.40	16.54	−9.82	−0.60	1.70	6.21	7.90	9.24	5.31
NGC 6402	M 14	21.32	14.81	3.9	0.60	16.61	−9.02	−1.39	1.60	33.24	9.07	9.36	3.30
NGC 6401		3.45	3.98	0.8	0.85	17.07	−7.62	−1.12	1.69	12.10	7.74	9.29	4.10
NGC 6397		338.17	−11.96	6.0	0.18	12.36	−6.63	−1.95	2.50c	15.81	4.90	8.46	5.68
NGC 6440		7.73	3.80	1.3	1.07	17.95	−8.75	−0.34	1.70	6.31	7.54	8.76	5.28
NGC 6441		353.53	−5.01	3.5	0.44	16.62	−9.47	−0.53	1.85	8.00	7.72	9.13	5.23
NGC 6453		355.72	−3.87	3.3	0.61	17.13	−7.05	−1.53	2.50c	21.50	6.87	8.36	4.72
NGC 6517		19.23	6.76	4.3	1.08	18.51	−8.28	−1.37	1.82	4.10	6.90	8.88	5.20
NGC 6522		1.02	−3.93	0.6	0.48	15.94	−7.67	−1.44	2.50c	16.44	6.32	8.90	5.31
NGC 6539		20.80	6.78	3.1	0.97	17.63	−8.30	−0.66	1.60	21.46	8.60	9.37	3.62
NGC 6540	Djorg 3	3.29	−3.31	4.4	0.60	14.68	−5.38	−1.20	2.50c	9.49	5.01	7.08	5.92
NGC 6544		5.84	−2.20	5.4	0.73	14.33	−6.56	−1.56	1.63c:	2.05	5.05	8.35	5.75
NGC 6569		0.48	−6.68	1.2	0.56	16.43	−7.88	−0.86	1.27	6.95	8.25	9.17	3.76

Table 2. continued.

ID	Name	l	b	R_{GC}	$E(B-V)$	$(m-M)_V$	M_{Vt}	[Fe/H]	c	r_t	$\log t_c$	$\log t_h$	$\log \rho_0$
NGC 6584		342.14	−16.41	7.0	0.10	15.95	−7.68	−1.49	1.20	9.37	9.01	9.09	2.92
NGC 6624		2.79	−7.91	1.2	0.28	15.37	−7.50	−0.42	2.50c	20.55	6.62	8.74	5.25
NGC 6638		7.90	−7.15	1.6	0.40	15.85	−6.83	−0.99	1.40	6.63	7.93	8.51	4.05
NGC 6637	M 69	1.72	−10.27	1.6	0.16	15.16	−7.52	−0.71	1.39	8.35	8.15	8.79	3.81
NGC 6642		9.81	−6.44	1.6	0.41	15.70	−6.57	−1.35	1.99	10.07	6.94	8.49	4.72
NGC 6652		1.53	−11.38	2.4	0.09	15.19	−6.57	−0.96	1.80	4.48	6.66	8.55	4.54
NGC 6681	M 70	2.85	−12.51	2.1	0.07	14.98	−7.11	−1.51	2.50c	7.91	5.62	8.83	5.41
NGC 6712		25.35	−4.32	3.5	0.45	15.60	−7.50	−1.01	0.90	7.44	8.86	8.98	3.14
NGC 6717	Pal 9	12.88	−10.90	2.3	0.20	14.95	−5.67	−1.29	2.07c:	9.87	6.61	8.26	4.65
NGC 6723		0.07	−17.30	2.6	0.05	14.87	−7.86	−1.12	1.05	10.51	8.99	9.30	2.81
NGC 6760		36.11	−3.92	4.8	0.77	16.74	−7.86	−0.52	1.59	12.96	7.94	9.39	3.84
NGC 6838	M 71	56.74	−4.56	6.7	0.25	13.75	−5.56	−0.73	1.15	8.96	7.64	8.41	3.05
NGC 6864	M 75	20.30	−25.75	12.8	0.16	16.87	−8.35	−1.32	1.88	7.28	7.85	9.08	4.51
NGC 6934		52.10	−18.89	14.3	0.09	16.48	−7.65	−1.54	1.53	8.37	8.43	9.07	3.37
NGC 6981	M 72	35.16	−32.68	12.9	0.05	16.31	−7.04	−1.40	1.23	9.15	8.93	9.20	2.35
NGC 7078	M 15	65.01	−27.31	10.4	0.10	15.37	−9.17	−2.25	2.50c	21.50	7.02	9.35	5.38
NGC 7089	M 2	53.38	−35.78	10.4	0.06	15.49	−9.02	−1.62	1.80	21.45	8.54	9.32	3.90
NGC 7099	M 30	27.18	−46.83	7.1	0.03	14.62	−7.43	-2.12	2.50c	18.34	6.38	8.95	5.04

lists were combined to create a raw color-magnitude diagram (CMD). First a catalog of mean magnitudes was created for each of the two filters, and then they were combined to obtain the $F439W-F555W$ colors. In this process, we used the programs DAOMATCH/DAOMASTER (kindly provided by P. B. Stetson), which yield magnitudes in the instrumental photometric system of the two $F555W$ and $F439W$ frames that were chosen as references.

2.3. The correction for CTE

In order to calibrate our photometry, we followed the procedure outlined in Dolphin (2000; D00). This accounts for both the charge transfer (in)efficiency (CTE) and the variation of the effective pixel area across the WFPC2 field of view, and it yields final calibrated magnitudes in either the Johnson photometric system or the HST one. As a first step, a softened background was calculated from the actual output of ALL-FRAME (after multiplying by the gain value $G = 7$ or 15, so counts are expressed in electrons) as follows. Negative values of the background were set to zero, and then the background counts (B) were replaced by $\sqrt{(1 + B^2)}$. The counts in electrons $D = G \times 10^{-0.4(m-25)}$ were then computed for each star magnitude. (Note that DAOPHOT sets a star magnitude to $m = 25$ for stars with a flux corresponding to one count above the sky background.) The B and D values were then used to find the CTE (and pixel area) correction to magnitude m, which is computed as $m = m - C$, where $C = Y + X$ and

$$X = \frac{x}{800}(0.024 + 0.002 \text{ yr})$$
$$\times \exp\left[-0.196(\ln D - 7) - 0.126(\ln B - 1)\right]$$

$$Y = \frac{y}{800}\Big\{0.018 + (0.097 + 0.041 \text{ yr})$$
$$\times (0.088 + \exp\left[-0.507(\ln D - 7)\right])$$
$$\times \exp\left[-0.035(\ln B - 1) - 0.042 \cdot B\right]\Big\}.$$

The CTE correction depends on the epoch of the observations (yr), which is expressed, in the D00 equations, relative to the reference epoch 1996.3. The coefficients of the equations were taken from Table 1 of D00, which is appropriate for observations made after April 23, 1994, when the camera was cooled from −76 °C to −88 °C. The corrected magnitudes were then calibrated to both the Johnson and HST flight systems, going through the steps described in the following Section.

2.4. Transformation to the standard photometric systems

The first step was to find the aperture corrections from ALLFRAME magnitudes to the reference aperture of 0.5″ used by Holtzman et al. (1995; H95). A set of bright isolated objects was selected, all their neighbors were subtracted, and aperture photometry was performed within the chosen set of radii. The aperture corrections were then defined as $AC = m_{PSF} - m_{0.5''}$, and median values were computed. Generally the agreement between the zero points of the four chips is good ($\Delta m < 0.01$ mag), but in some cases the procedure gave poor aperture corrections. This normally happened for the more crowded PC chip. In such cases, the aperture corrections were changed by a few hundredths of a magnitude in order to bring the PC photometry into agreement with the WF zero points. This procedure will of course erase any true magnitude offset introduced by a patchy reddening on arcmin scales, so we warn the

readers that these data are not suitable for mapping the reddening within the sky area covered by the WFPC2.

Once the aperture corrections had been applied, the following procedure was followed. First, the aperture corrections AC_{555} and AC_{439}, and the absorptions A_{555} and A_{439} were subtracted from the instrumental magnitues. Since the absorptions depend on the true colors, which are not known at the beginning, we started with null values for A_{555} and A_{439}. From the corrected instrumental magnitudes m_{555} and m_{439} the counts were computed in the usual way, i.e., $D_{555} = 10^{-0.4(m_{555}-25)}$ and $D_{439} = 10^{-0.4(m_{439}-25)}$. The D values were used to compute the provisional flight magnitudes, as given by the D00 equations:

$$F555W = -2.5\log(D_{555}/t_{555}) + 21.734 + \Delta Z_{CG}$$

$$F439W = -2.5\log(D_{439}/t_{439}) + 20.086 + \Delta Z_{CG}.$$

In these equations, t_{555} and t_{439} are the exposure times in seconds, the filter- and temperature-dependent zero-points were taken from Table 6 of D00 (Cold Z_{FG} column), and the chip to chip zero-point differences ΔZ_{CG} were in turn taken from Table 5. Explicitly, for gain 7 the values are $0.701, 0.761, 0.749$, and 0.722 for the PC, WF2, WF3 and WF4 chips, respectively. For gain 15 the values are, in the same order of chips, -0.044, $0.007, -0.007$, and -0.005.

The determination of the Johnson B and V magnitudes is complicated by the fact that they depend on the true color of the star, so we followed an iterative procedure. Assuming $B - V = 1$, we computed the provisional magnitudes as prescribed by D00:

$$V = F555W - 0.060 \times (B - V) + 0.033 \times (B - V)^2$$

$$B = F439W + 0.003 \times (B - V) - 0.088 \times (B - V)^2.$$

We then computed an updated value of $B - V$ and iterated until the difference between successive values of the magnitudes dropped below 0.001.

At this stage we are still ignoring absorption. However, we now have an estimate of the Johnson magnitudes, so we can compute a first provisional value of A_{555} and A_{439}. They can be subtracted, together with the aperture corrections, from the instrumental magnitudes, and the previous cycle can be repeated until new values for the absorptions are obtained. Indeed, the cycle was repeated until again the differences between successive values of V and B were smaller than 0.001.

The absorptions were computed in the following manner. The absorptions for two stars of spectral type K5 and O6 are given in H95 for the different HST filters, as a function of the reddening E_{B-V}. In order to compute the absorption for a star of any spectral type, two fiducial $B - V$ colors were assigned to the two reference types, $B - V = 1.15$ and $B - V = -0.32$, respectively. The absorptions for stars of intermediate colors were computed as linear interpolations between the values at the two color extremes. Since the range in color of our stellar populations is not extreme, the same linear interpolation was used also to compute the absorptions for stars falling outside the preferred color range. The average reddening of each globular cluster was taken from the Harris (1996) catalog.

In practice, it is impossible to directly compare the photometry of the data base published in this paper with any photometric catalog from groundbased data. Our HST images are on the central, very crowded regions which are not the usual targets of groundbased investigations. An indirect check of the photometric calibration is shown in Fig. 3, where the HB magnitude levels of the HST CMDs and of the CMDs from two groundbased photometric datasets are compared. The (*upper panel*) shows the differences between the V magnitudes of the horizontal branch (V_{HB}) of Rosenberg et al. (1999) and the V_{HB} for a subsample of our clusters (De Angeli 2001; Piotto et al. 2002), as a function of the reddening. In the *lower panel*, our V_{HB} are compared with the corresponding values tabulated by Harris (1996). The V_{HB} for the HST data have been derived as in Zoccali et al. (1999). There is a good agreement between the HST and groundbased values.

2.5. Artificial star experiments and completeness

In order to correct the empirical star counts for completeness, we performed standard artificial star experiments for each GGC. In order to optimize the cpu time, in our experiments we tried to add the largest possible number of artificial stars in a single test, without artificially increasing the crowding of the original field, i.e., avoiding the overlap of two or more artificial-star profiles. To this purpose, as described in Piotto & Zoccali (1999), the artificial stars were added in a spatial grid such that the separation of the centers in each star pair was two PSF radii plus one pixel. The relative position of each star was fixed within the grid. However, the grid was randomly moved on the frame for each different experiment.

For each artificial star test, the frame-to-frame coordinate transformations (as calculated from the original photometry) were used to ensure that the artificial stars were added exactly in the same position in each frame. We started by adding stars in one V frame at random magnitudes; the corresponding B magnitude for each star was chosen according to the fiducial points representing the instrumental CMD. The frames obtained in this way were processed following the same procedure used for the reduction of the original images.

The completeness fraction, typically in 0.4 mag intervals, was then computed as the ratio between the number of the added artificial stars and the number of artificial stars found in the same magnitude range.

We performed separate experiments for the HB, the subgiant and red giant branches, and the blue stragglers and main sequence. In each of the three CMD branches, we ran 8 independent experiments for each of the 4 WFPC2 chips, adding in each experiment 600 stars in the PC camera and 700 stars in the WF camera, for a total of more than 7100 experiments, with more than 5 million artificial stars added.

A comparison between the added magnitudes and the measured magnitudes allows us also a realistic estimate of the internal photometric error, defined as the standard deviation of the differences between the magnitudes added and those found, as a function of magnitude.

Table 3. Example of a photometry file (NGC 104, 47 Tuc): Col. 1 gives a star identification number, Cols. 2 and 3 give the position on the chip, Cols. 4 and 5 the V and B standard magnitudes (reddening corrected), Cols. 6 and 7 the $F555W$ and $F439W$ magnitudes in the HST flight system (reddening corrected), Cols. 8 and 9 the photometric errors given by ALLFRAME, Cols. 10 and 11 the V and B standard magnitudes (before the reddening correction), Cols. 12 and 13 the $F555W$ and $F439W$ flight magnitudes (before the reddening correction), Cols. 14 and 15 the χ and sharp parameters as given by ALLFRAME, and Col. 16 the chip number (1 for PC, and 2, 3, 4 for WF2, WF3, WF4 respectively).

ID	x	y	V	B	$F555W$	$F439W$	σ_{F555W}	σ_{F439W}
4	506.598	59.980	17.97	18.74	18.00	18.79	0.10	0.10
7	200.220	60.927	18.94	19.28	18.96	19.29	0.24	0.08
8	235.644	61.244	16.49	17.15	16.52	17.19	0.15	0.07
9	545.239	61.390	14.68	15.62	14.70	15.70	0.08	0.04
5	688.846	61.697	21.49	21.90	21.51	21.91	0.26	0.43
15	736.285	61.745	19.66	20.30	19.68	20.34	0.15	0.10
5603	537.317	62.062	18.96	19.48	18.99	19.50	0.16	0.08
12	445.775	62.208	18.65	19.37	18.67	19.42	0.09	0.06
14	636.699	62.301	18.00	18.65	18.02	18.69	0.08	0.06
11	119.039	62.725	17.59	18.03	17.61	18.04	0.09	0.06

V_{nr}	B_{nr}	$F555W_{nr}$	$F439W_{nr}$	χ	sharp	chip
18.13	18.94	18.16	19.00	2.206	0.046	1
19.09	19.49	19.11	19.50	1.821	−0.032	1
16.65	17.35	16.67	17.39	6.213	0.157	1
14.83	15.82	14.86	15.90	9.128	0.040	1
21.64	22.10	21.66	22.12	1.015	−0.282	1
19.81	20.51	19.84	20.55	1.421	−0.041	1
19.12	19.68	19.14	19.71	2.239	0.162	1
18.80	19.57	18.83	19.62	1.677	0.079	1
18.15	18.85	18.18	18.90	2.230	0.108	1
17.75	18.23	17.77	18.25	1.887	−0.032	1

An example of the completeness functions, and of the internal photometric errors obtained from the artificial star experiments is shown in Fig. 2. We have selected two typical situations: (a) the case of a high central density cluster (NGC 104), and (b) the case of a low density object (NGC 6723).

3. The database

Figures 4 show the final CMDs for the 74 GGCs of our database in the $F439W$ and $F555W$ HST flight system. Note that the magnitude and color ranges covered by each figure are always of the same size (though magnitude and color intervals are different), with the exception only of NGC 6397. Typically from a few thousands to about 47 000 (e.g. in NGC 6388) stars have been measured in each cluster.

Table 3 shows an example of the final photometric file.

After the publication of the present paper, all the CMDs, the star positions, the magnitudes in both the $F439W$ and $F555W$ flight system and the B and V standard Johnson system can be retrieved from the Padova Globular Cluster Group Web pages at `http://menhir.pd.astro.it`[1]. We will also make available the star-count completeness results of the single clusters,

upon request to the first author. Anyone who uses the photometric data retrieved from the Web pages and the completeness corrections is kindly asked to cite the present paper.

In the file that gives the photometry we have included two sets of magnitudes in each of four photometric bands. We give magnitudes in the HST flight system ($F439W$, $F555W$), and the Johnson B and V magnitudes that result from the iterative procedure that uses the Harris (1996) reddening subtraction, as described in Sect. 2.4. We also give magnitudes in both systems before the reddening correction: ($F439W_{nr}$, $F555W_{nr}$) and (B_{nr}, V_{nr}). In general we would advise the reader to use the $F439W_{nr}$ and $F555W_{nr}$ magnitudes (Cols. 12 and 13). If one needs to work in the Johnson system for highly reddened clusters, however, the only magnitudes which can be safely used are the B and V magnitudes resulting from the iterative calibration procedure (Cols. 4 and 5), though we cannot guarantee that the adopted reddening is correct.

---

[1] Note that this address will become `http://dipastro.pd.astro.it/globulars` in the near future.
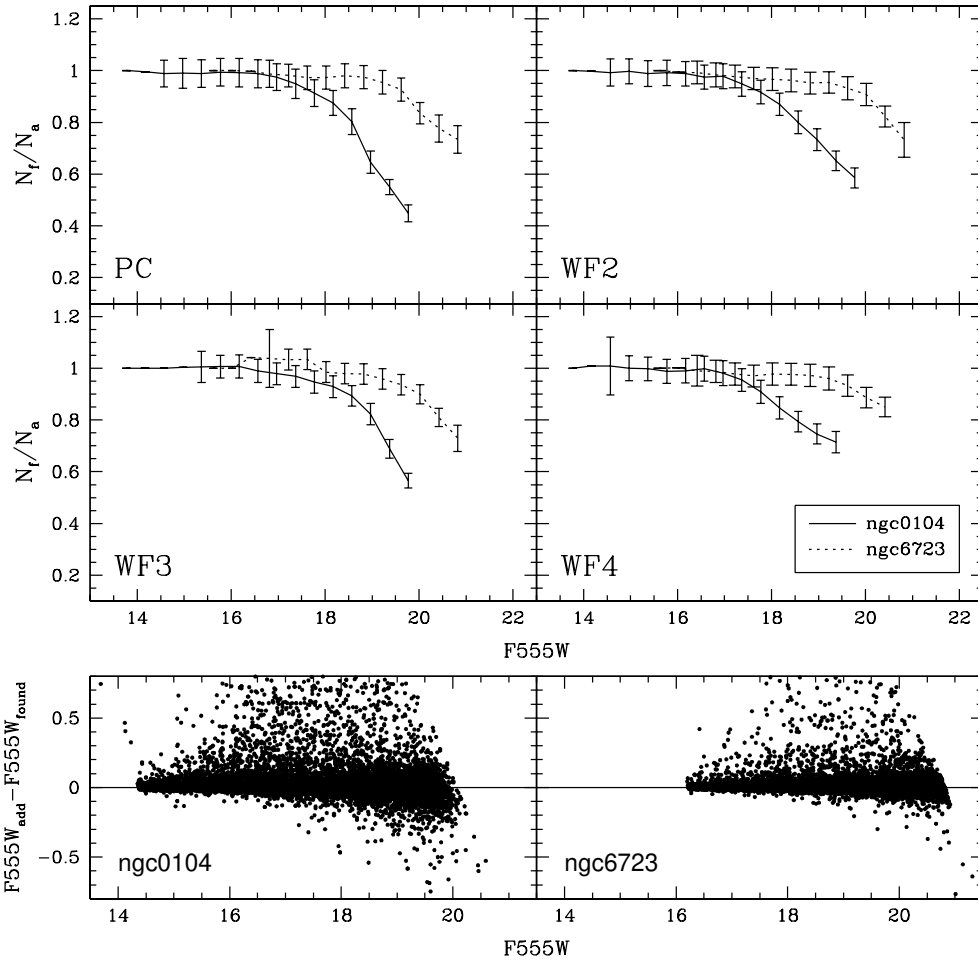
Fig. 2. Completeness functions and internal photometric errors from the artificial star experiments for the case of a high central density cluster (NGC 104), and of a low density object (NGC 6723).
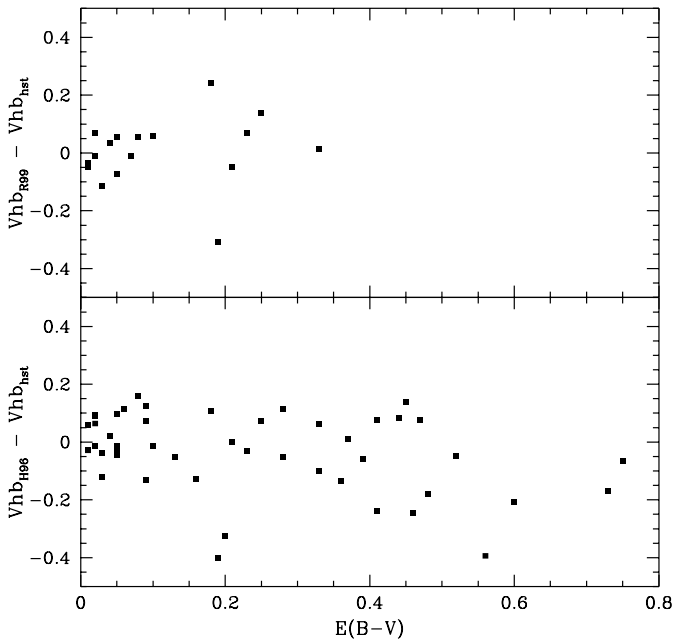
Fig. 3. *Upper panel*: differences between the magnitude level of the HB (V_{HB}) of Rosenberg et al. (1999) and the V_{HB} for a subsample of our clusters (De Angeli 2001; Piotto et al. 2002) as a function of reddening. *Lower panel*: differences between the V_{HB} of Harris (1996) and the V_{HB} of a subsample of our clusters.
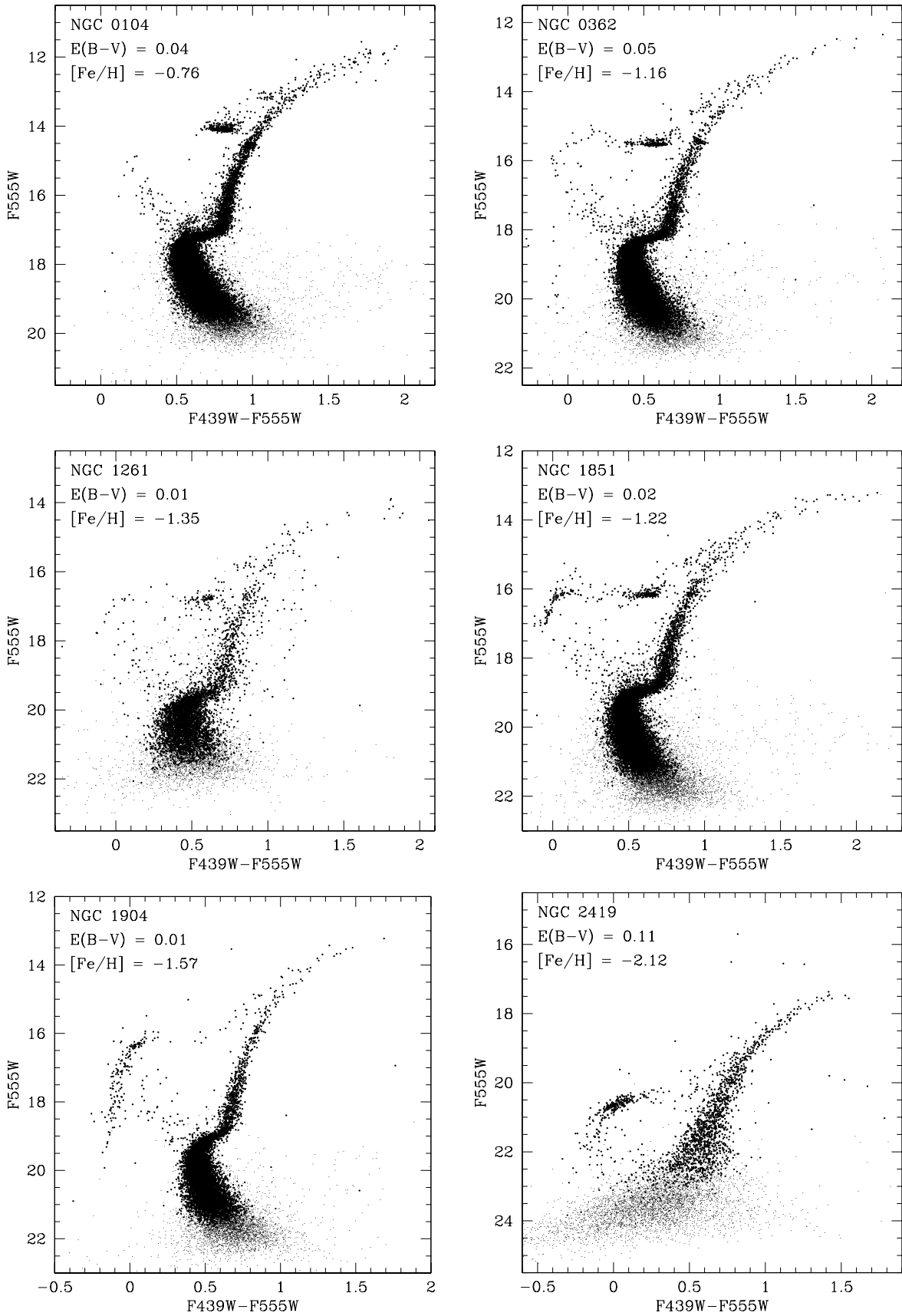
Fig. 4. The *F*555*W* vs. *F*439*W*−*F*555*W* (flight system) color magnitude diagrams from the combination of the 4 WFPC2 cameras of 2 clusters of the database. Note that the magnitude and color ranges covered by each figure are always of the same size (though magnitude and color intervals start at different values). Heavier dots correspond to stars with an internal total error less than 0.1 mag.
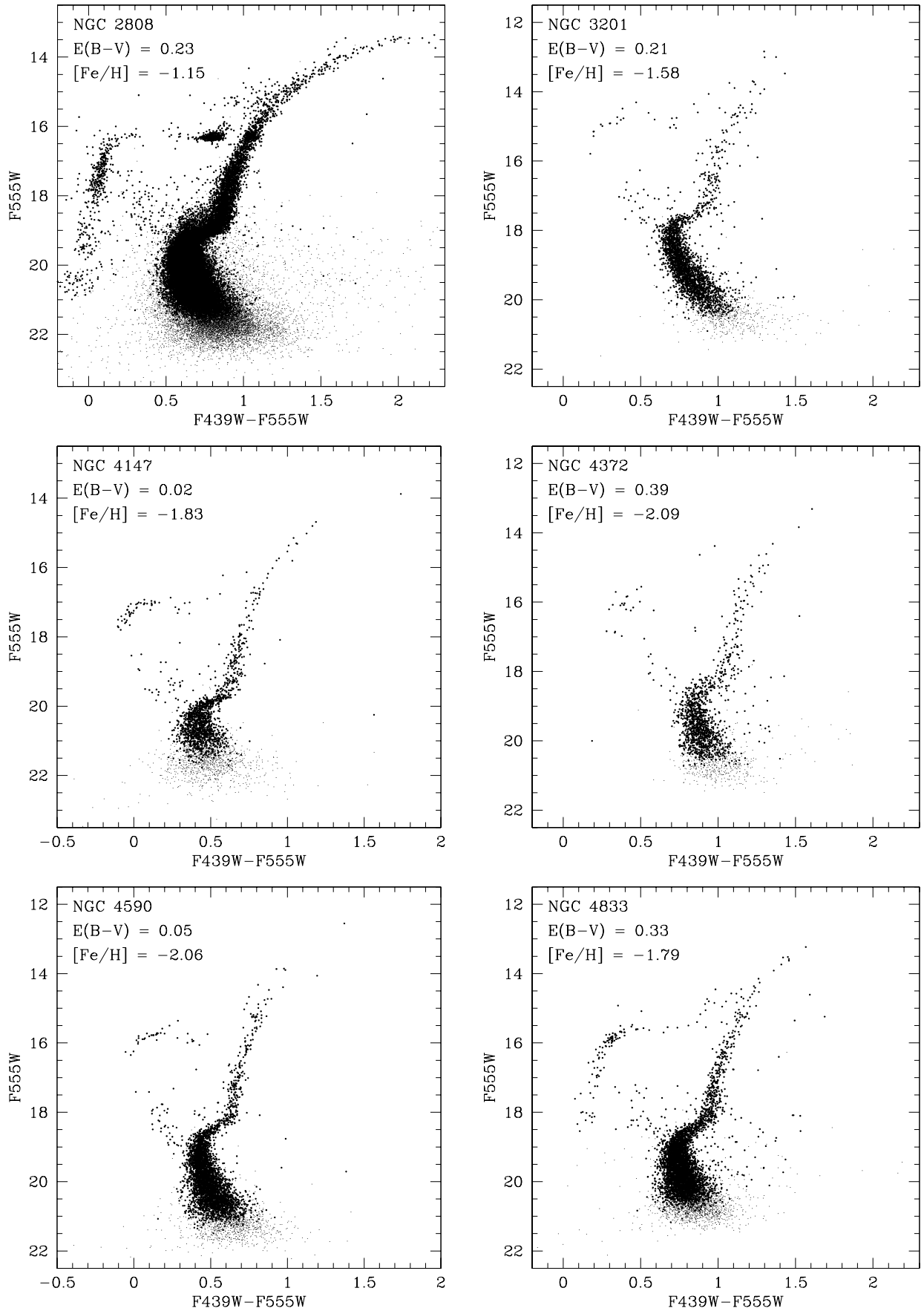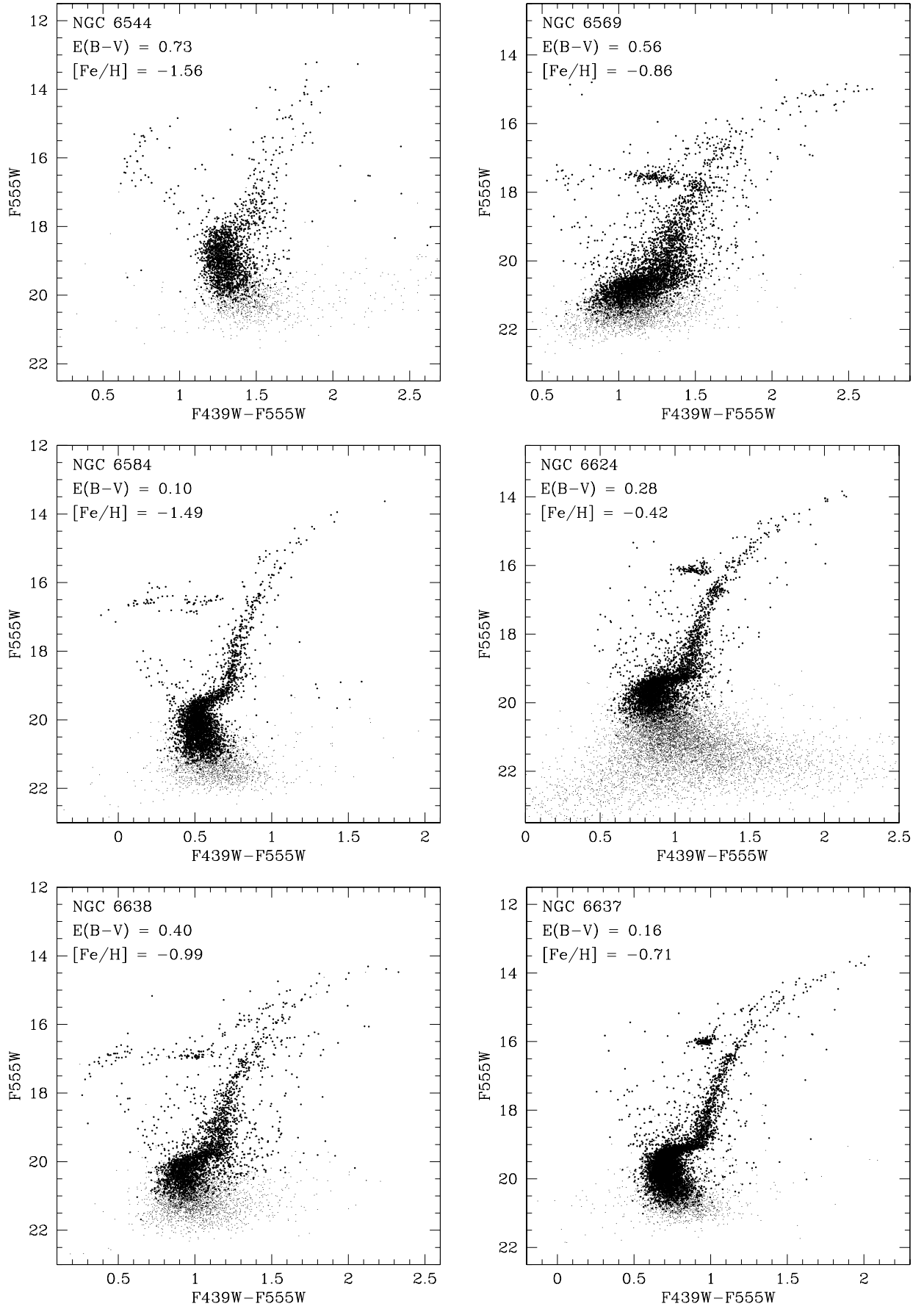
Fig. 4. continued.
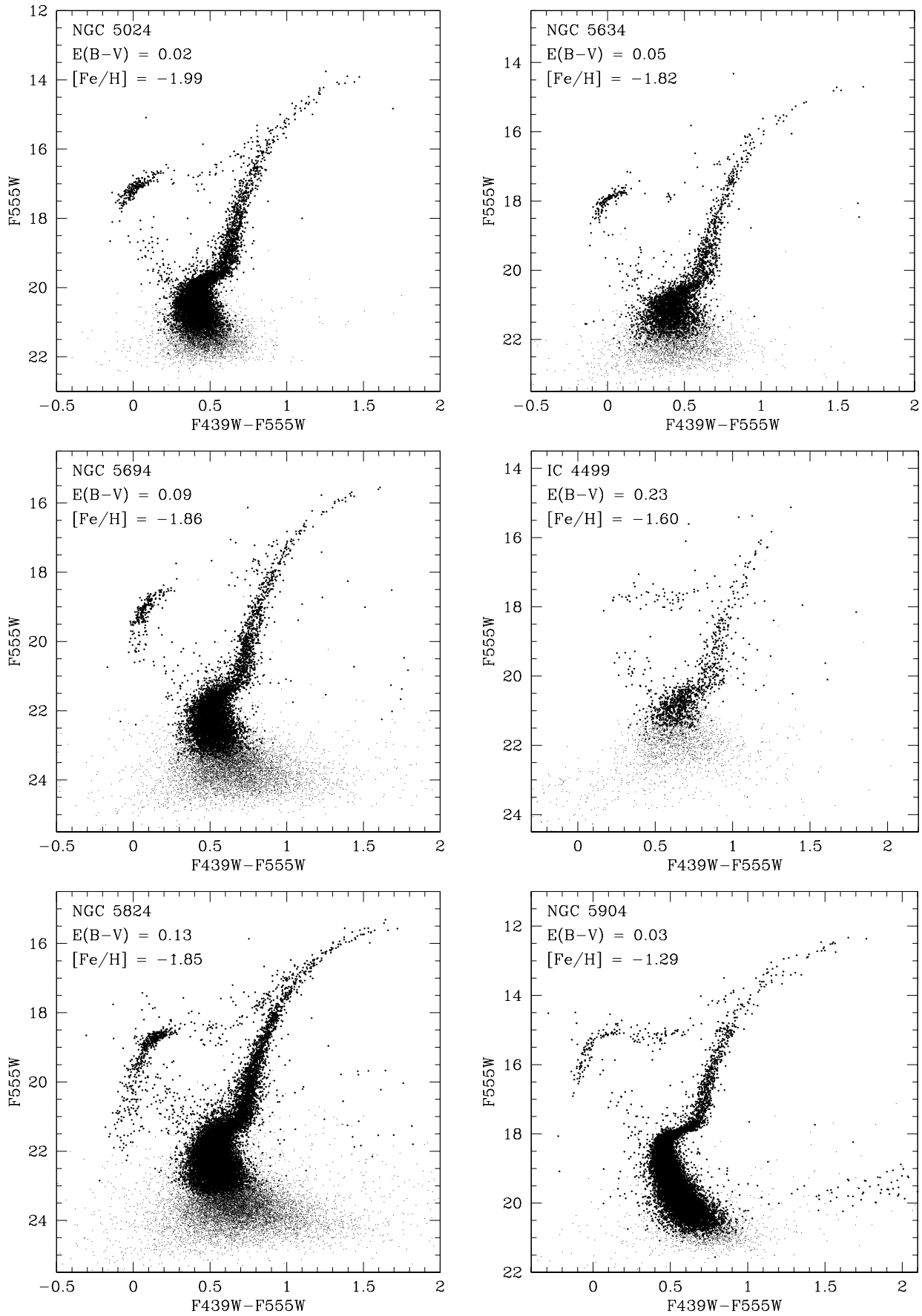
Fig. 4. continued.
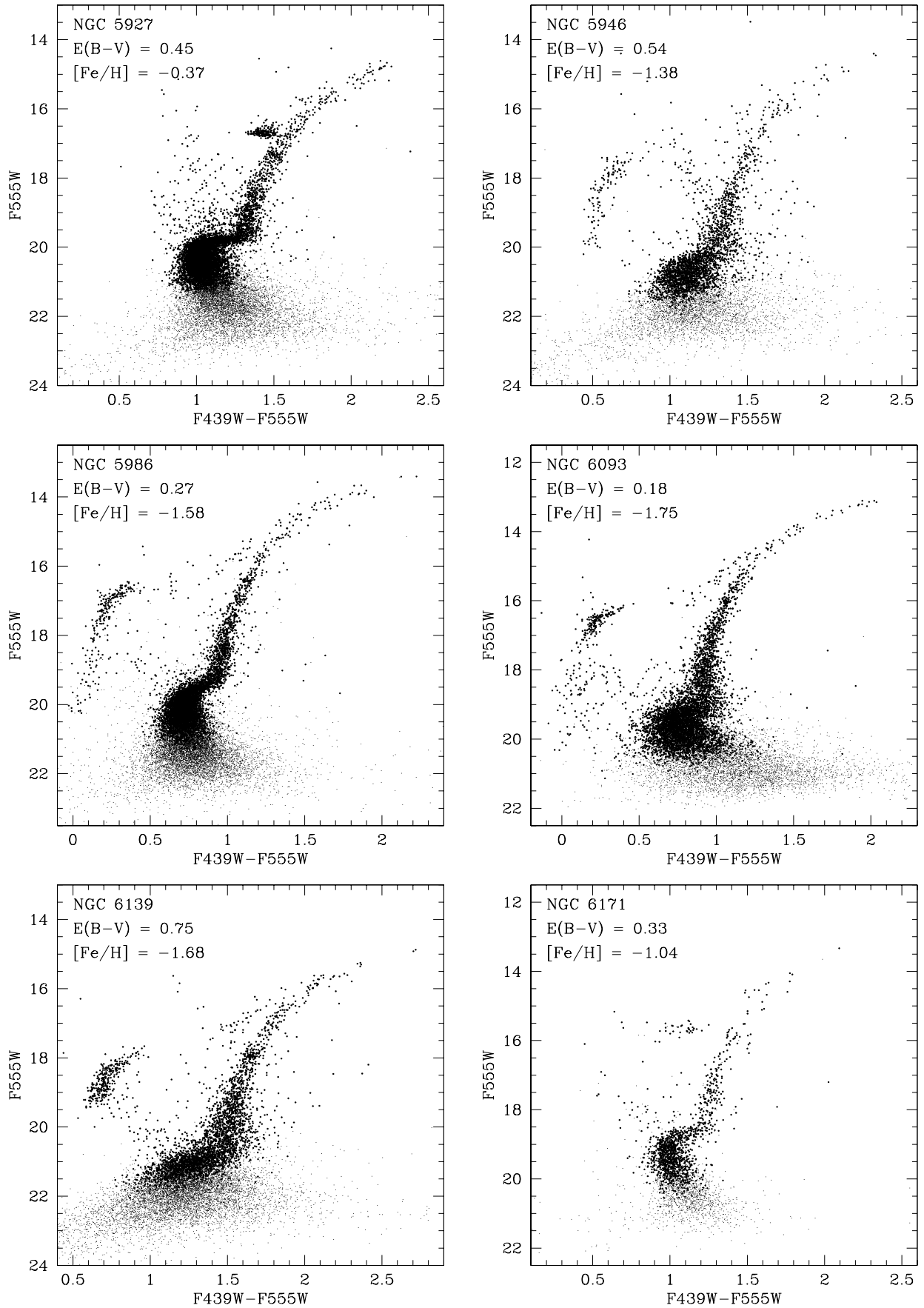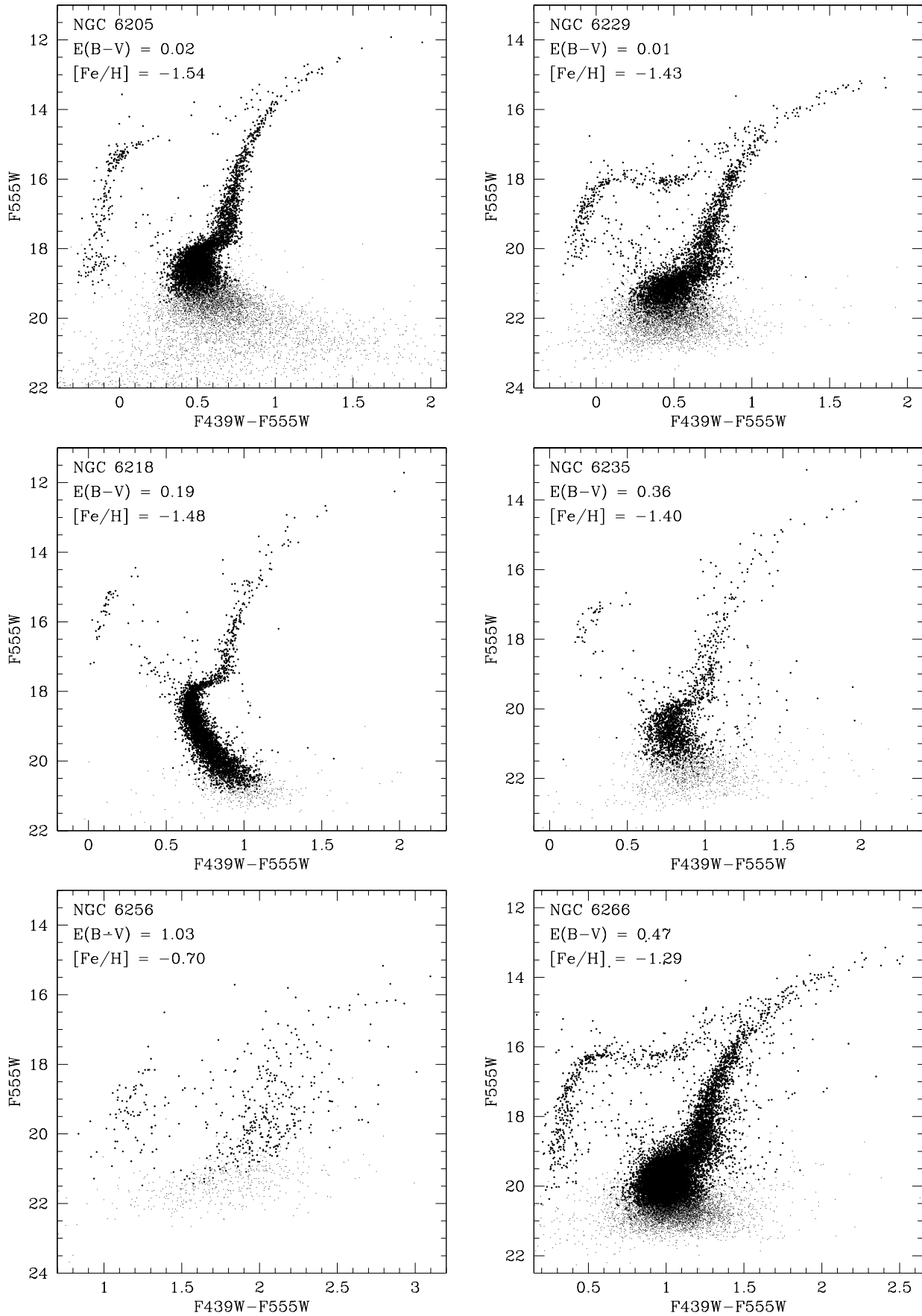
Fig. 4. continued.
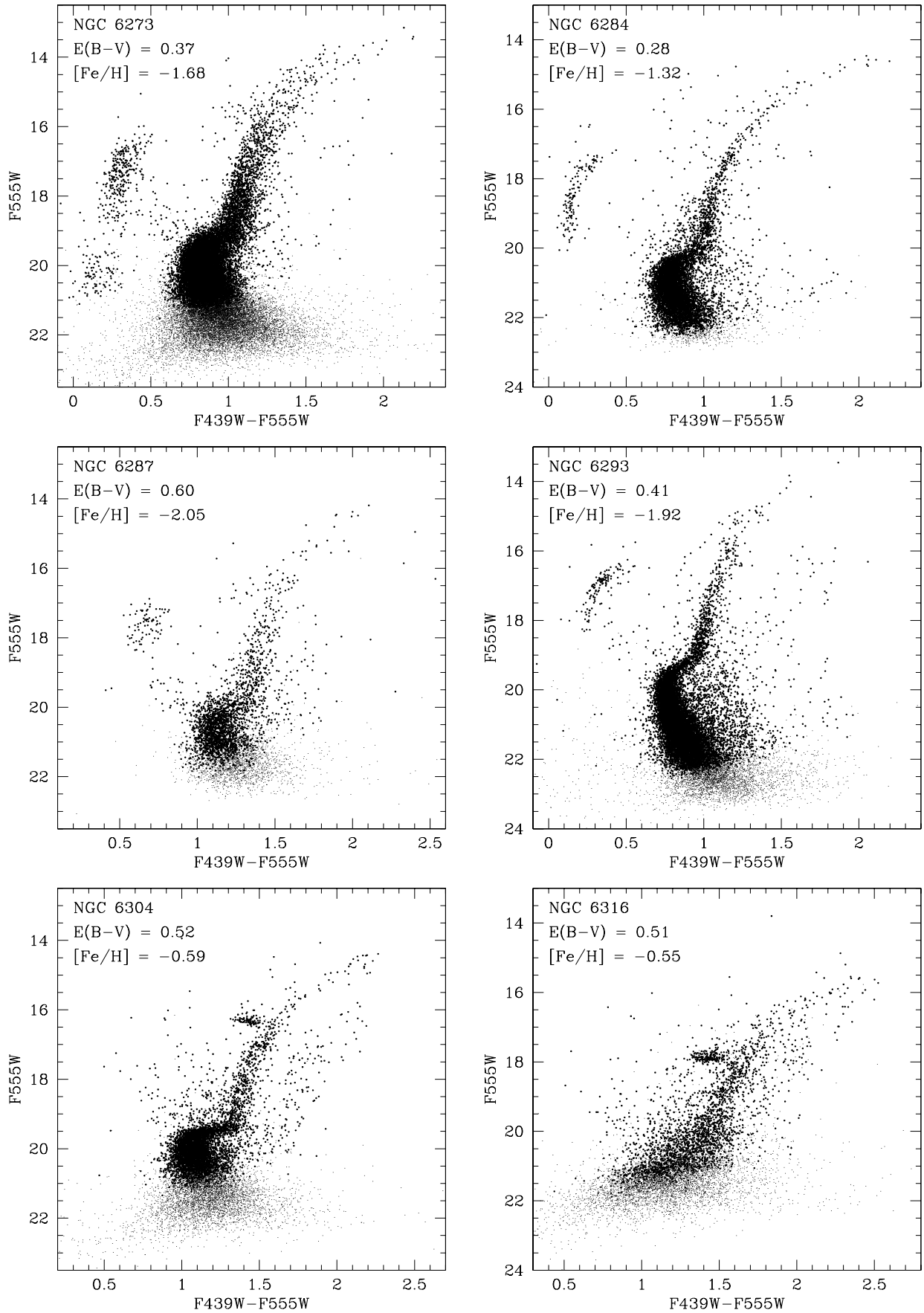
Fig. 4. continued
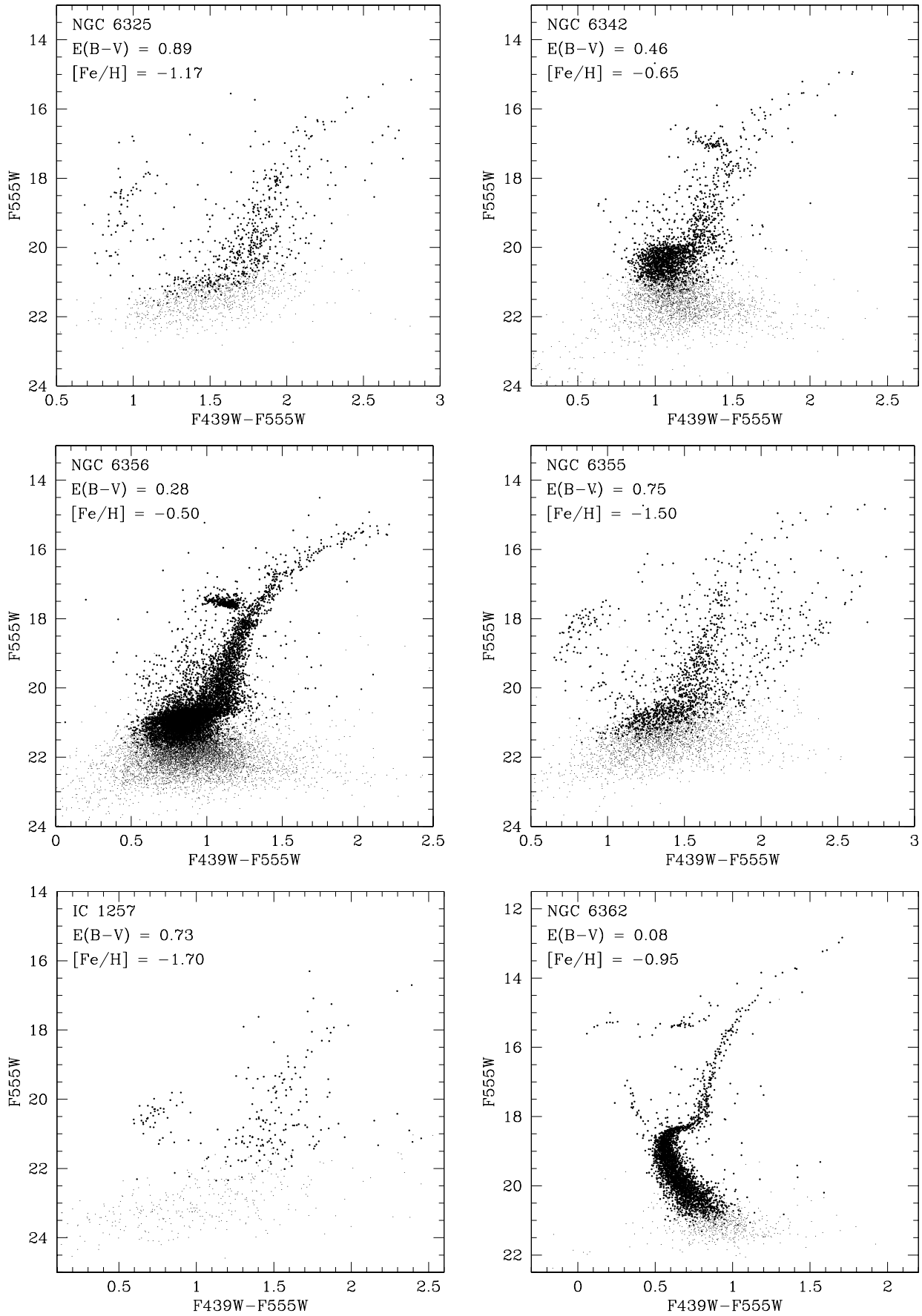
Fig. 4. continued.
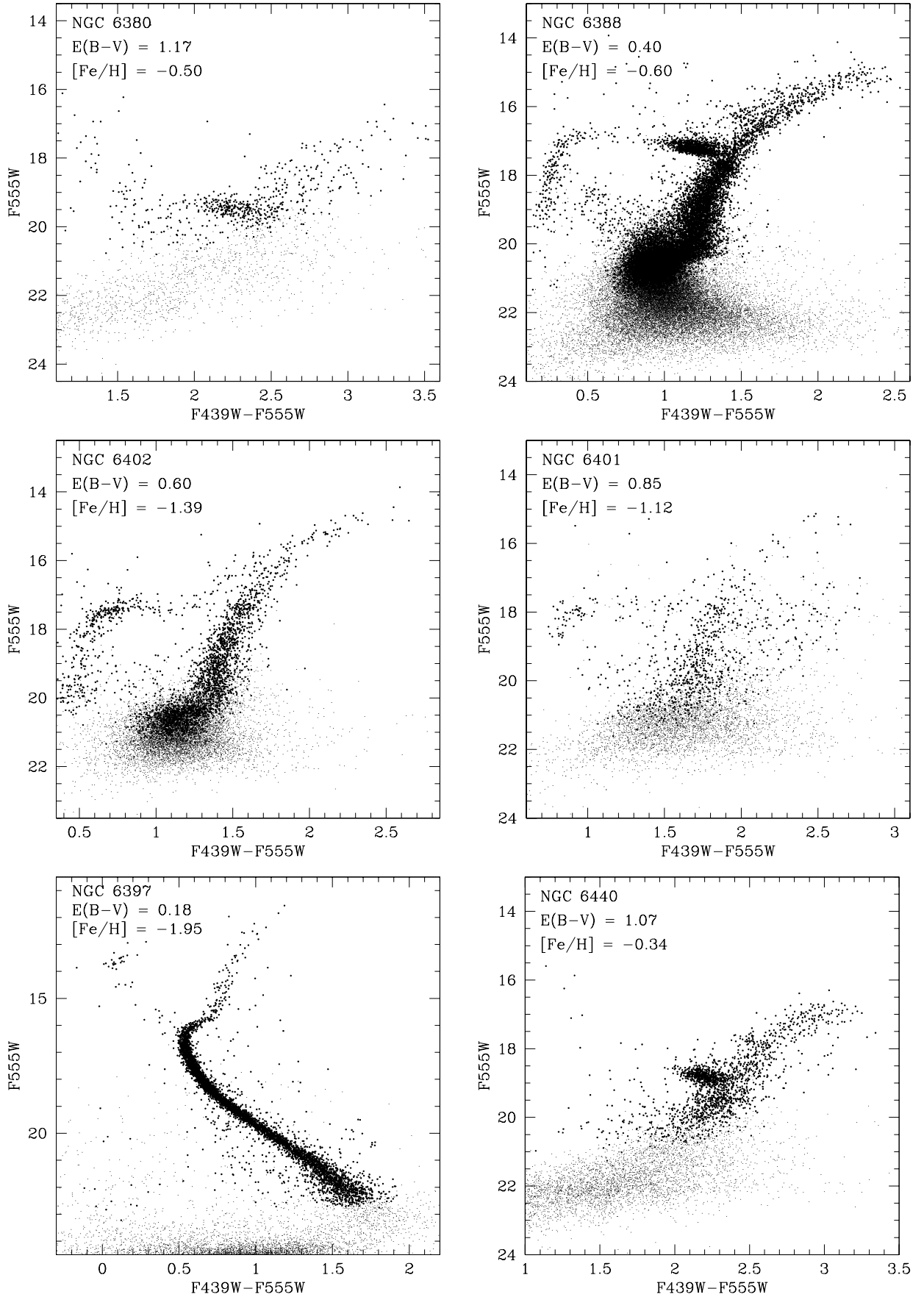
Fig. 4. continued
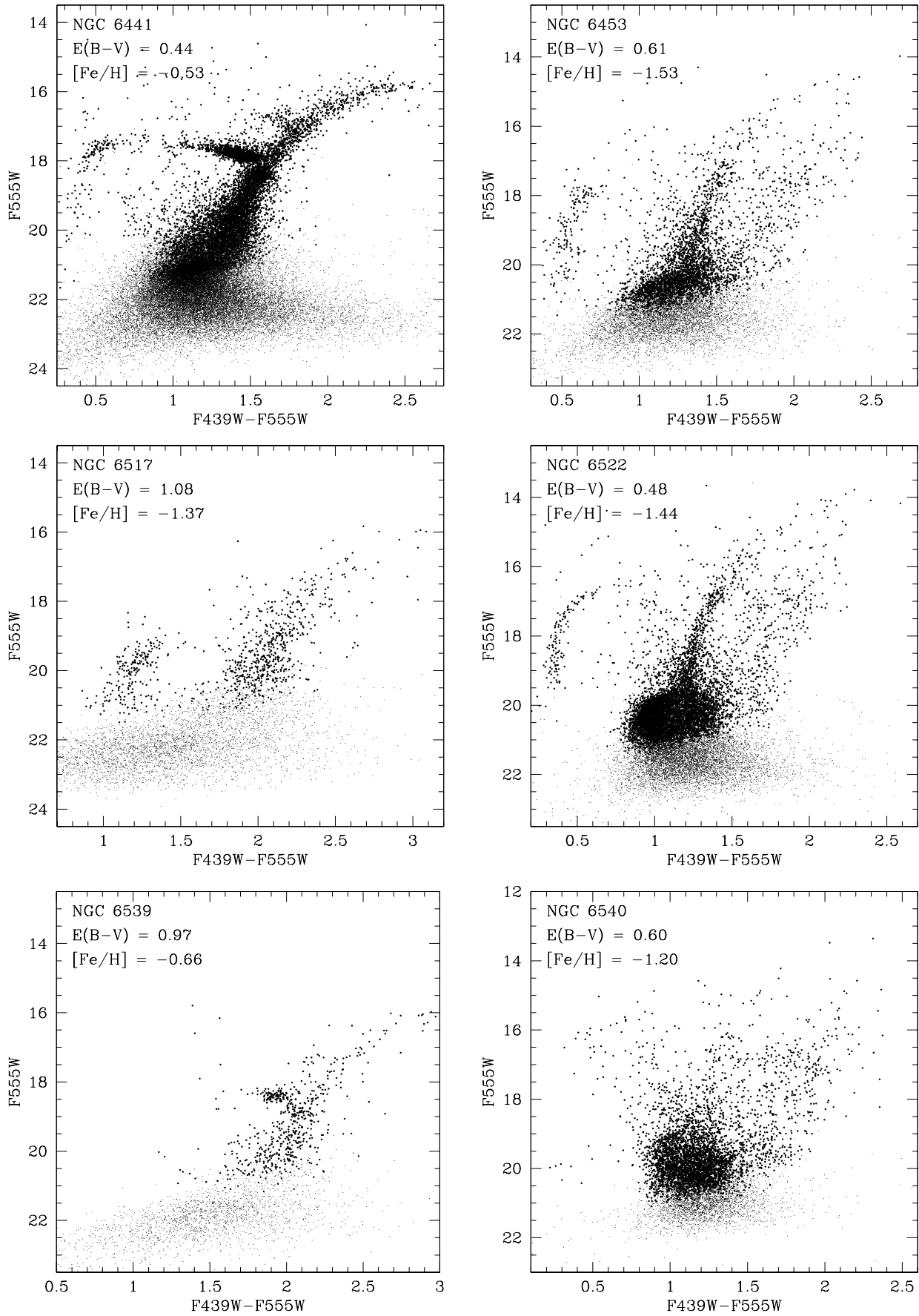
Fig. 4. continued.

Fig. 4. continued. Note that the magnitude range of the CMD for NGC 6397 differs from the other cases.
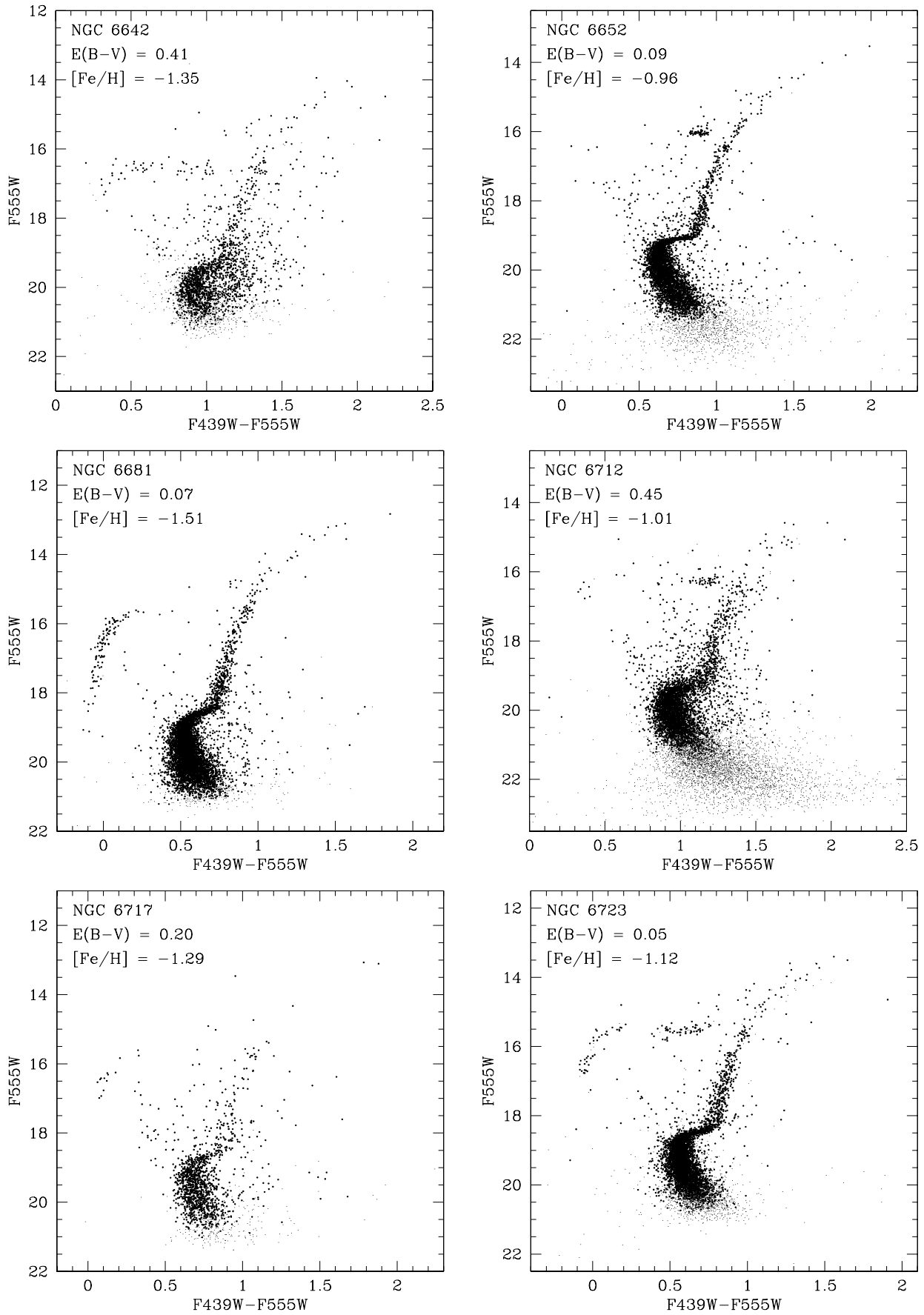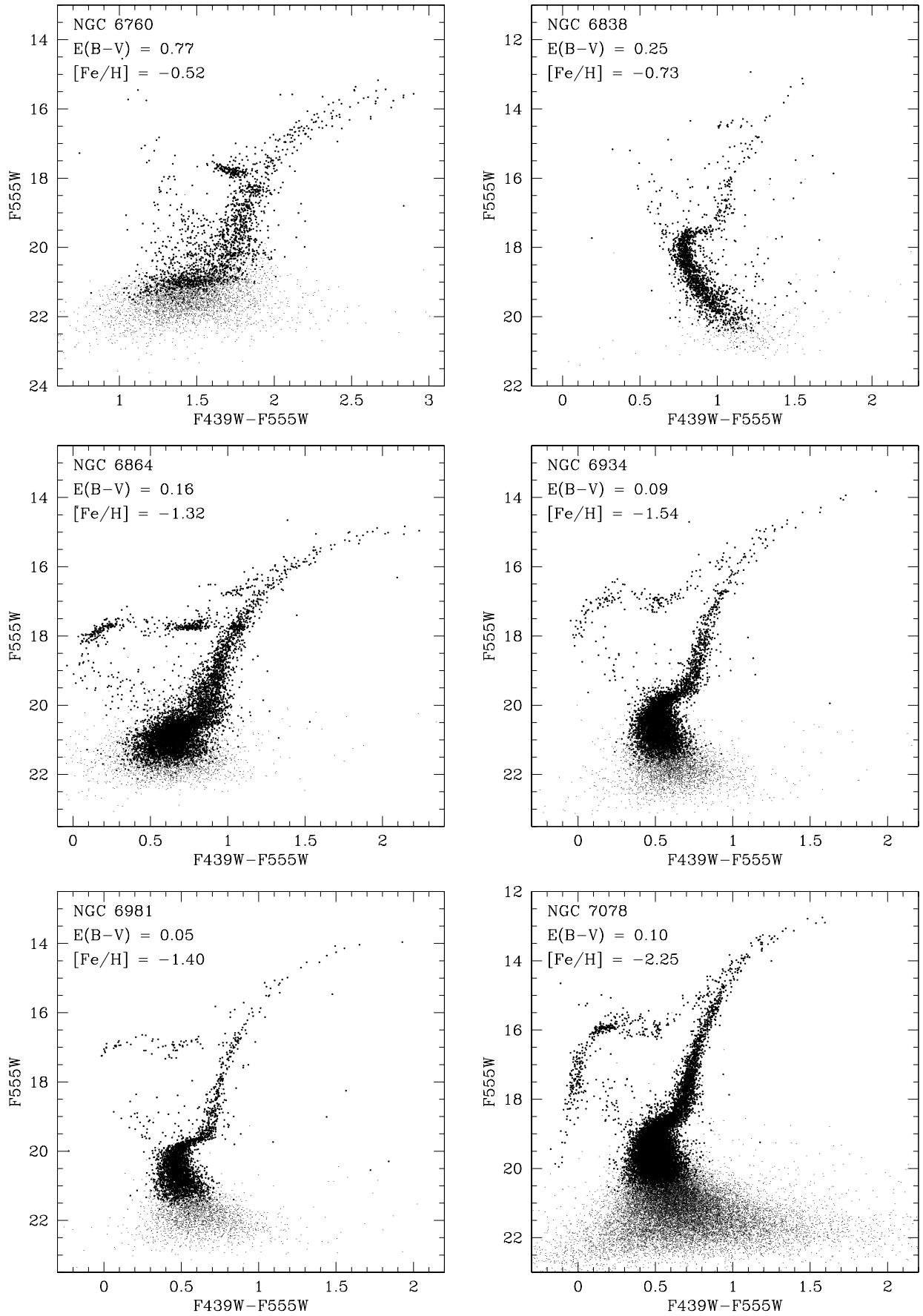
Fig. 4. continued.

Fig. 4. continued.

Fig. 4. continued.

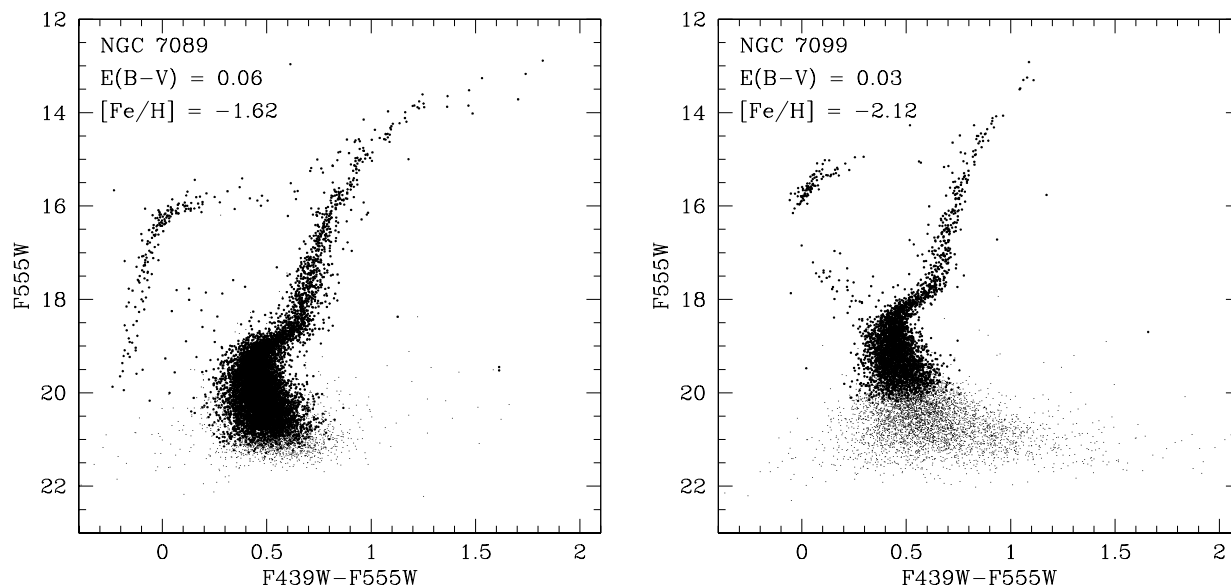**Fig. 4.** continued.

References

Bono, G., Cassisi, S., Zoccali, M., & Piotto, G. 2001, ApJ, 546, L109

Cassisi, S., Castellani, V., Degl'Innocenti, S., Piotto, G., & Salaris, M. 2001, A&A, 366, 578

De Angeli, F. 2001, Tesi di Laurea, Università di Padova

Dolphin, A. E. 2000, PASP, 112, 1397 (D00)

Harris, W. E. 1996, AJ, 112, 1487

Holtzman, J. A., Burrows, C. J., Casertano, S., et al. 1995, PASP, 107, 1065 (H95)

Piotto, G., Sosin, C., King, I. R., et al. 1997, in Advances in Stellar Evolution, ed. R. T. Rood & A. Renzini (Cambridge: Cambridge University Press), 84

Piotto, G., Zoccali, M., King, I. R., et al. 1999a, AJ, 117, 264

Piotto, G., Zoccali, M., King, I. R., et al. 1999b, AJ, 118, 1727

Piotto, G., & Zoccali, M. 1999, A&A, 345, 485

Piotto, G., Rosenberg, A., Saviane, I., Aparicio, A., & Zoccali, M. 2000, The Galactic Halo: From Globular Cluster to Field Stars, 471

Piotto, G., De Angeli, F., Djorgovski, S., et al. 2002, in preparation

Raimondo, G., Castellani, V., Cassisi, S., Brocato, E., & Piotto, G. 2002, ApJ, in press [astro-ph0201123]

Rich, R. M., Sosin, C., Djorgovski, S. G., et al. 1997, ApJ, 484, L25

Rosenberg, A. R., Saviane, I., Piotto, G., & Aparicio, A. 1999, AJ, 118, 2306

Silbermann, N. A., Harding, P., Madore, B. F., et al. 1996, ApJ, 470, 1

Sosin, C., Piotto, G., King, I. R., et al. 1997a, in Advances in Stellar Evolution, ed. R. T. Rood, & A. Renzini (Cambridge: Cambridge Univ. Press), 92

Sosin, C., Dorman, B., Djorgovski, S. G., et al. 1997b, ApJ, 480, L35

Stetson, P. B. 1987, PASP, 99, 191

Stetson, P. B. 1994, PASP, 106, 250

Zoccali, M., Cassisi, S., Piotto, G., Bono, G., & Salaris, M. 1999, ApJ, 518, L49

Zoccali, M., Cassisi, S., Bono, G., et al. 2000, ApJ, 538, L289

Zoccali, M., & Piotto, G. 2000, A&A, 358, 943